Functional evaluation of novel soluble insulin-like growth factor (IGF)-II–specific ligand traps based on modified domain 11 of the human IGF2 receptor

Stuart N. Prince,[1] Emily J. Foulstone,[1] Oliver J. Zaccheo,[1] Christopher Williams,[2] and Andrew Bassim Hassan[1]

[1]Molecular Oncology and Growth Factor Cancer Research UK Group, Department of Cellular and Molecular Medicine, School of Medical Sciences and [2]Department of Biological and Organic Chemistry, School of Chemistry, University of Bristol, Bristol, United Kingdom

Abstract

Ligands transported by the mannose 6-phosphate/insulin-like growth factor (IGF)-II receptor (IGF2R) include IGF-II– and mannose 6-phosphate–modified proteins. Increased extracellular supply of IGF-II, either secondary to loss of the clearance function of IGF2R, loss of IGF binding protein function, or increased *IGF2* gene expression, can lead to embryonic overgrowth and cancer promotion. Reduced supply of IGF-II is detrimental to tumor growth, and this suggests that gain of function of IGF-II is a molecular target for human cancer therapy. Domain 11 of IGF2R binds IGF-II with high specificity and affinity. Mutagenesis studies have shown that substitution of glutamic acid for lysine at residue 1554 results in a 6-fold higher affinity for IGF-II (20.5 nmol/L) than native domain 11 (119 nmol/L). Here, we generate a novel high-affinity IGF-II ligand trap by fusion of mutated human 11^{E1554K} to a COOH-terminal human IgG1 Fc domain (11^{E1554K}-Fc). The resulting homodimer has a significantly increased affinity for IGF-II (1.79 nmol/L) when measured by surface plasmon resonance. IGF-II signaling via the IGF-I receptor and the proliferative effect of IGF-II were specifically inhibited by 11^{E1554K}-Fc in both HaCaT and *Igf2*$^{-/-}$ mouse embryonic fibroblast cells. These data confirm that a novel engineered and soluble IGF2R-11^{E1554K}-Fc protein functions as an IGF-II–specific and high-affinity ligand trap *in vitro* and that this protein has potential application as an IGF-II antagonist for cancer therapy following *in vivo* experimental evaluation. [Mol Cancer Ther 2007;6(2):607–17]

Introduction

Insulin-like growth factor (IGF)-II (7.5 kDa) has significant homology to IGF-I and both exert their growth effect through the IGF-I tyrosine kinase receptor [IGF-I receptor (IGF1R)], leading to phosphorylation of signaling molecules, including mitogen-activated protein kinase (MAPK), protein kinase B (PKB)/AKT, mammalian target of rapamycin, FOXO transcription factors, glycogen synthase kinase-3β, and MDM2, combining to promote growth and antiapoptotic signaling (1, 2). Both IGFs can also bind the insulin receptor and hybrids of the insulin and IGF1Rs, with IGF-II binding particularly to isoform A of the insulin receptor, resulting in stimulation of insulin signaling pathways (3).

Unlike IGF-I, the potent growth-promoting functions of IGF-II occur principally during embryonic growth and in tumors where there is increased supply due to disruption of regulatory mechanisms (2, 4). In mammals, the tight regulation of IGF-II extracellular bioavailability is achieved by high-affinity binding to six extracellular IGF binding proteins (proteins 1–6), with IGF binding protein proteolytic cleavage during development and in tumors leading to increased local free ligand supply and IGF1R activation (5–7). Mutation of IGF1R has not been frequently detected in tumors, but protein overexpression has been observed and is associated with malignant cellular transformation in some instances (8, 9). Genetic disruption and transgene overexpression of *Igf2* in several murine models of tumor susceptibility have established the role of the ligand in tumor progression following initiating mutations (10–17). Moreover, IGF-II supply is commonly increased within high-grade human cancers, including hepatocellular, breast, prostate, colorectal, ovarian, and sarcoma (18–23).

Increased supply of IGF-II can also occur following loss of imprinting of the gene, leading to biallelic expression and embryonic overgrowth (2). Loss of imprinting of *IGF2* has been described in many tumor types, including pediatric solid tumors (24–26) and carcinomas (27, 28), and is particularly associated with increased relative risk of developing colorectal carcinoma (27, 29). In IGF-II–overexpressing tumors, deregulated IGF-II proprotein processing can also lead to delivery of high molecular weight forms of IGF-II that retain the E peptide (30). Increased circulating levels of big IGF-II produced by tumors can lead to activation of the insulin receptor and cause nonislet cell tumor-induced hypoglycemia (30).

Received 8/18/06; revised 11/17/06; accepted 12/21/06.

Grant support: Cancer Research UK grant C429.

The costs of publication of this article were defrayed in part by the payment of page charges. This article must therefore be hereby marked *advertisement* in accordance with 18 U.S.C. Section 1734 solely to indicate this fact.

Note: S.N. Prince and E.J. Foulstone equally contributed to this work.

Requests for reprints: Andrew Bassim Hassan, Weatherall Institute for Molecular Medicine, University of Oxford, John Radcliffe Hospital, Headington, Oxford OX3 9DS, United Kingdom. Phone: 01865-222440; Fax: 01865-222431. E-mail: bass.hassan@cancer.org.uk

doi:10.1158/1535-7163.MCT-06-0509

IGF-II not bound to intact IGF binding protein may also bind and be cleared by the mannose 6-phosphate/IGF-II receptor (IGF2R), a 270-kDa P-type lectin that exists in both transmembrane (type 1) and soluble forms (31–33). IGF2R functions include binding and sequestering IGF-II for degradation, trafficking lysosomal enzymes and mannosylated proteins to and from the prelysosomal compartment, and activation of transforming growth factor-β1 (31, 33, 34). Of the 15 homologous extracellular domains, only domain 11 directly binds IGF-II with domain 13 important for high-affinity binding (10^{-10} mol/L; refs. 35, 36). *IGF2R* loss of heterozygosity and mutations occur frequently in common cancers, such as hepatocellular (70%), breast (40%), and cancers associated with mismatch repair defects, and *IGF2R* is proposed to be a tumor suppressor gene (37–40).

The crystal structure of domains 1, 2, 3, and 11 of the human IGF2R have been determined (41, 42). All domains have a similar topology that consists of a flattened barrel formed by nine β-strands. This structure is shared with the cation-dependent mannose 6-phosphate receptor (14–28% identity) and avidin (43). The crystal structure of domain 11 has been determined at 1.4Å resolution using the anomalous scattering of sulfur, although no structural alignments with IGF-II have yet been determined (42). Domain 11 is characterized by two hydrophobic binding sites, the first being a shallow cleft that is located at the mouth of the barrel and the second being a region that extends along an external flattened surface. The former binding cleft volume (400 $Å^3$) is formed by loops AB, CD, and FG (42). Mutation of the solvent-exposed residues in this region (AB loop: Y1542, S1543, and G1546; CD loop: F1567, G1568, T1570, and I1572; and FG loop: S1596, P1597, and P1599) followed by real-time analysis of affinity has led to the identification of CD loop residues as essential for the initial hydrophobic docking with IGF-II (44). In addition, AB loop residues seem to act as second sphere residues that stabilize the interaction (44). Moreover, mutation of E1544 to alanine, lysine, arginine, and histidine significantly enhanced the affinity of domain 11 to IGF-II (44).

Here, we sought to exploit our structural and functional knowledge of IGF2R domain 11 to design a functional IGF-II ligand trap that could have therapeutic potential as a soluble IGF-II–specific antagonist.

Materials and Methods

Materials

Restriction enzymes and CIAP were purchased from New England Biolabs, Inc. (Hichin, United Kingdom). The BIAcore 3000 biosensor, HBS-EP buffer, SA sensor chips, and BIAevaluation software were from BIAcore, Inc. (Uppsala, Sweden). Oligonucleotides were purchased from MWG-Biotech (Ebersberg, Germany). *Drosophila* D.Mel-2 cells and medium, the *Drosophila* expression vector pMT/BiP/V5-His B, DMEM/F-12 (1:1), and fetal bovine serum were purchased from Invitrogen (Paisley, United Kingdom). Amicon Ultra filters were from Millipore (Watford, United Kingdom). Recombinant human IGF-I and IGF-II were from GroPep (Adelaide, South Australia, Australia). Anti–phospho-(Ser^{473}) PKB and anti–phospho-p44/42 MAPK (Thr^{202}/Tyr^{204}) antibodies were from Cell Signaling Technology (Danvers, MA). Enhanced chemiluminescence and protein affinity purification reagents were from Amersham Biosciences (Little Chalfont, United Kingdom). Unless otherwise stated, all other reagents were purchased from Sigma (Poole, United Kingdom).

Production of Monomeric Domain 11 Proteins in *Pichia Pastoris*

Wild-type (WT) domain 11, enhanced mutant 11^{E1544K}, and null mutant 11^{I1572A} proteins were produced in *Pichia Pastoris* as described previously (44). Briefly, stable transformants were cultured at 300 rpm in 200 mL BMGY medium overnight at 30°C, then pelleted, and transferred to 200 mL BMMY medium for 3 days with 1% methanol added daily. The media were made according to Invitrogen recipes. Supernatants were concentrated using 10-kDa MWCO Centricon-Plus 70 filters. 6× His-tagged proteins were affinity purified using nickel sepharose (Sigma). Buffer exchange into PBS and protein concentration was done using 10-kDa MWCO Amicon Ultra-15 filters.

Construction of Fc-Tagged IGF-II Ligand Trap Expression Vectors

Domain 11 of M6P/IGF2R cDNA was PCR amplified from plasmid pEFBOS_1-15 (36) using Pwo polymerase (Roche, Burgess Hill, United Kingdom) and the *Bgl*II site containing forward primer Bgl-11-forward (5′-AAAAAAAA*GATCT*CCCATGAAGAGCAACGAGCATGAT-3′) and the *Age*I site containing reverse primer Age-11-reverse (5′-AAAA*ACCGGT*GCAGGCCAGCGGCGTGTG-3′). The PCR product was desalted using Microcon YM-100 filters (Millipore) and digested with the restriction enzymes *Bgl*II and *Age*I. The digested PCR product was gel purified using Geneclean (QBiogene, Cambridge, United Kingdom) and cloned into *Bgl*II and *Age*I double-digested, gel-purified *Drosophila* expression vector pMT/BiP/V5-His B to create pDes11. This construct was then COOH-terminally tagged with the human IgG1 Fc domain as a dimerization motif. To achieve this, Fc domain cDNA was PCR amplified from IMAGE clone 4851063 (ATCC-6878978) using Pwo polymerase and the *Age*I site containing primers Age-Fc-forward (5′-AAAA*ACCGGT*GAGCCCAAATCTTCTGACAAAACTC-3′) and Age-Fc-reverse (5′-AAAA*ACCGGT*TTTTACCCGGAGACAGGGAGAGG-3′) according to rationale described previously (45). The PCR product was cleaned with a Microcon YM-100, digested with *Age*I, purified by Geneclean, and cloned into *Age*I-digested and CIAP-dephosphorylated pDes11 to create pDes11-Fc. Orientation of the cloned Fc gene was determined by PCR using the Bgl-11-forward and Age-Fc-reverse primers. To facilitate the future cloning of 11-Fc into other expression vectors, the *Age*1 site linking domain 11 to the Fc tag was removed using the Stratagene (La Jolla, CA) ExSite mutagenesis kit and the 5′ phosphorylated oligonucleotides Fc ExSite forward (5′-GAGCCCAAATCTTCTGACAAAACTCACAC-3′) and 11 ExSite reverse (5′-TTCGGTCGCTTGCTCGCAGG-3′). Site-directed null and enhanced mutant versions of domain 11 were made using the oligonucleotides and protocols

described previously (i.e, 11^{E1544K} and 11^{I1572A}; ref. 44). Fc-tagged domain 11^{I1572A} (null mutant) and Fc-tagged domain 11^{E1544K} (enhanced mutant) expression vectors were thus generated and named pDes11^{I1572A}-Fc and pDes11^{E1544K}-Fc, respectively. All constructs were verified by DNA sequencing, done by the University of Dundee Sequencing Service. The proteins produced from these vectors were named 11-Fc, 11^{I1572A}-Fc, and 11^{E1544K}-Fc.

Production of Fc-Tagged IGF-II Ligand Trap Proteins in *Drosophila* Melanogaster Cells

D.Mel-2 serum-free adapted *Drosophila melanogaster* Schneider 2 cells were maintained in 5 mL *Drosophila*–serum-free medium supplemented with 16.5 mmol/L L-glutamine, at 28°C in T-10 tissue culture flasks. The cells were seeded at 1×10^5 per mL and split when they reached 1×10^7 per mL. Cells were transfected at 70% confluency in a T-175 flask by complexing 48 μg pDes11-Fc plasmid DNA with 96 μL Transfectin reagent (Bio-Rad, Hemel Hemstead, Herts, United Kingdom) according to the manufacturer's instructions. Transfected cells were cultured in 30 mL of medium total. Twenty-four hours post-transfection, 30 μL of 500 mmol/L filter-sterilized copper sulphate were added to induce transgene expression. The cells were maintained in culture for a further 72 h to secrete folded protein expressed from the transgene. Sodium phosphate was then added to the cell supernatant to a final concentration of 20 mmol/L and the pH was adjusted to 7. The supernatant was filter sterilized and Fc-tagged protein was affinity purified with 3 mL ProteinA FastFlow Sepharose (Amersham Biosciences) in a column according to the manufacturer's instructions. Bound protein was washed with five column volumes of 20 mmol/L sodium phosphate (pH 7) and eluted in five column volumes of 0.1 mol/L sodium citrate (pH 3.5). The eluted protein was rapidly neutralized with 0.1 volume of 1 mol/L Tris (pH 9), and the pH was adjusted to 7.4. Buffer exchange into PBS and protein concentration was done using 30-kDa MWCO Amicon Ultra-15 filters. The column was regenerated with 0.1 mol/L sodium citrate (pH 3) and stored in 20% ethanol.

Measurement of Protein Size and Purity

The absorbance at 280 nm of purified protein was measured, protein concentration was calculated using the extinction coefficient, and mass was determined by the ProtParam tool available on the ExPASy.org Web site.[3] Fc-tagged proteins expressed in *Drosophila* cells are *N*-glycosylated with two 982.9-Da molecules of $Man_3GlcNAc_2$ (46), and so this was included in the mass calculation. Purified protein was filter sterilized and stored at 4°C in aliquots. Protein samples were denatured and electrophoresed by SDS-PAGE and visualized by Coomassie staining against Precision markers (Bio-Rad).

Analytic Gel Filtration (Fast Protein Liquid Chromatography)

To further purify proteins and measure their native mass, fast protein liquid chromatography was used as described previously (44). For the Fc-tagged proteins, fast protein liquid chromatography analytic gel filtration was carried out on a Superdex 200 HR 10/30 column (Amersham Biosciences) equilibrated with 10 mmol/L HEPES (pH 7.4), 150 mmol/L NaCl, and 3 mmol/L EDTA and linked to an ÄKTA Purifier system (Amersham Biosciences). The column was calibrated with amylase (200 kDa), alcohol dehydrogenase (150 kDa), bovine serum albumin (66 kDa), carbonic anhydrase (29 kDa), and cytochrome *c* (12.5 kDa). Purified protein was loaded at ~5 mg/mL. The molecular weights of the proteins were determined from a plot of the Ve/Vo versus log (molecular weight) of the standards, where Ve is the elution volume of the protein and Vo is the void volume. The void volume for the column was determined by the elution of blue dextran (2,000 kDa).

Surface Plasmon Resonance Experiments

Surface plasmon resonance analysis of protein binding to IGF-II was done using a BIAcore 3000 biosensor. Biotinylated IGF-II (GroPep, Adelaide, South Australia, Australia) was immobilized to the surface of one flow cell in a streptavidin-coated BIAcore SA sensor chip to a level of 50 resonance units. Biotinylated IGF-I (GroPep) was immobilized to a level of 50 resonance units on a separate flow cell. Kinetic binding experiments for Fc-tagged IGF2R domain 11 proteins were carried out at 25°C at a 75 μL/min flow rate in HBS-EP binding buffer. For kinetic assays, six concentrations of Fc-tagged IGF2R domain 11 protein were prepared by doing 2-fold serial dilutions (in HBS-EP) ranging from 2.464 to 0.077 nmol/L. A buffer control and a reference flow cell were included. Analytes were injected over the ligand surface for 3 min, following which the analyte solutions were replaced by HBS-EP buffer for 1 h. Regeneration of the sensor chip for subsequent injections was accomplished by a 60 μL injection of 2 mol/L $MgCl_2$. All experiments were repeated in triplicate. Data transformation and overlay plots were prepared with BIAevaluation software version 4.0.1. The reference flow cell data were subtracted and the regeneration and air spikes were deleted. Curves were x and y transformed and the buffer control was subtracted. Data were fitted simultaneously and as much association and dissociation data were included as possible. Injection start and stop points were set precisely and the data fit using the bivalent analyte model for curve fitting without bulk refractive index change. Mass transfer control experiments were done by injecting 0.616 nmol/L 11^{E1544K}-Fc protein at five flow rates: 5, 20, 40, 60, and 75 μL/min. Binding curves were compared for consistency.

Cell Culture

HaCaT human keratinocytes, a kind gift from Dr. A. Hague (Department of Oral and Dental Science, University of Bristol, Bristol. United Kingdom), were grown in DMEM/F-12 (1:1) supplemented with 10% fetal bovine serum, 0.5 μg/mL hydrocortisone, 50 IU/mL penicillin, 5 μg/mL streptomycin, and 1 mmol/L L-glutamine. Immortalized $Igf2^{-/-}$ mouse embryonic fibroblasts (MEF) were derived by us from E14 embryos ($Igf2^{-/-}$) using estab lished procedures. Briefly, the embryo was washed in PBS,

[3] http://expasy.org/

the head and liver were removed, and the embryo was disaggregated with forceps, and cells were allowed to grow out to form a monolayer. These cells were immortalized using the 3T3 method (47). Cells were grown in DMEM supplemented with 10% fetal bovine serum, 50 IU/mL penicillin, 5 μg/mL streptomycin, and 1 mmol/L L-glutamine. All cells were maintained at 37°C in 5% carbon dioxide with humidity.

Western Blot Signaling Analysis

Twenty-four hours after seeding onto six-well plates (1×10^5 cells per well), cells were serum starved overnight before stimulation. IGFs and domain 11 constructs were preincubated as appropriate in serum-free medium at room temperature for 10 min before placing on the cells for a further 10 min. After stimulation, cells were washed twice with ice-cold PBS and immediately scraped into 100 μL lysis buffer [50 mmol/L Tris-HCl (pH 7.5), 1% NP40, 1 mmol/L EDTA, 120 mmol/L NaCl, 40 mmol/L β-glycerophosphate, 1 mmol/L benzamidine, 1 mmol/L NaF, 1 mmol/L Na_3VO_4, 1 mmol/L phenylmethylsulfonyl fluoride, 1 μg/mL leupeptin, 1 μg/mL antipain, 1 μg/mL pepstatin]. Insoluble material was removed by centrifugation and proteins were separated under reducing conditions on 12% SDS-PAGE and transferred to polyvinylidene difluoride membrane (Millipore) before detection with anti–phospho-(Ser^{473}) PKB or anti–phospho-p44/42 MAPK (Thr^{202}/Tyr^{204}) antibodies following the manufacturer's instructions. Proteins were visualized using enhanced chemiluminescence reagents. Equal protein loading was verified using an anti–α-tubulin antibody (Sigma).

[^{3}H]thymidine Incorporation Assay

Cells were seeded onto 24-well plates (HaCaT, 1×10^4 cells per well; MEFs, 3×10^4 cells per well) in growth medium. After 24 h, HaCaT cells were serum starved for 24 h and then treated with appropriate IGF and domain 11 constructs preincubated at room temperature in 500 μL serum-free medium for 10 min. After a further 24 h, 1 μCi [^{3}H]thymidine per well was added, and the cells were incubated for 1 h. Medium was removed and cells were washed twice with PBS before fixation in 500 μL of 5% Trichloroacetic acid for 20 min at 4°C followed by extraction in 400 μL of 0.1 mol/L NaOH at 4°C for 1 h. MEFs were serum starved overnight before stimulation with appropriate IGF, and domain 11 constructs were preincubated in 500 μL of serum-free medium at room temperature for 10 min. [^{3}H]thymidine (1 μCi) per well was added with the IGFs, and cells were incubated for 24 h before fixation in 5% TCA and extraction with 0.1 mol/L NaOH. Incorporation of [^{3}H]thymidine was analyzed by scintillation counting.

Statistical Analysis

Data were analyzed with the Student's *t* test (Minitab version 14 software, Minitab, Inc., College Station, PA).

Results

In this study, we have generated human IgG1 Fc domain COOH-terminally tagged fusion proteins of the WT, enhanced (11^{E1544K}), and null (11^{I1572A}) mutant forms of IGF2R domain 11 (Fig. 1A). These constructs were expressed in *Drosophila* D.Mel-2 cells and secreted into the serum-free growth medium at a concentration of 10 mg/L. A summary of the calculated physical properties of the native Fc-tagged and untagged domain 11 proteins is shown in Table 1. A denaturing Coomassie brilliant blue–stained gel of the purified proteins (Fig. 1B) showed that proteins ran as a single band and that their denatured masses were very close to those predicted. Analytic gel filtration revealed that the native Fc-tagged domain 11 proteins were dimeric and eluted as a single peak at 13.58 mL (Fig. 1C) with a mass (86 kDa), close to the predicted mass (88.06 kDa; see Table 1).

Affinity of Fc-Tagged Domain 11 Proteins for IGF-II

The affinity of versions of Fc-tagged domain 11 fusion proteins, and domain 11 constructs, for IGF-II were compared using surface plasmon resonance (BIAcore 3000). Immobilization of biotinylated IGF-I and IGF-II on separate flow cells of a streptavidin-coated sensor chip (BIAcore) generated reproducible sensorgram profiles when Fc-tagged and untagged domain 11 proteins were passed over the surface as analytes (Fig. 2A and B). The IGF-II binding kinetics of the monomeric domain 11 proteins (WT and 11^{E1544K}) have been published by us and are only shown here for comparison (Fig. 2A; ref. 44). The Fc-tagged domain 11 kinetic data done in triplicate generated sensorgrams that were analyzed using a bivalent analyte model (Fig. 2B). Global fits of the data with a bivalent analyte model without bulk refractive index change, generated no χ^2 >1.94 and provided optimal fits to the data. As with the control monomeric domain 11 null mutant (11^{I1572A}), the 11^{I1572A}-Fc homodimer had no affinity for either IGF-II or IGF-I. Moreover, neither Fc-tagged WT domain 11 (11-Fc) nor Fc-tagged enhanced mutant domain 11 (11^{E1544K}-Fc) had an affinity for IGF-I (data not shown), confirming that dimerization had not altered ligand specificity. From the sensorgrams for IGF-II binding (Fig. 2B), it was apparent that 11-Fc and 11^{E1544K}-Fc both had high affinity for IGF-II, with resonance units responses for 11^{E1544K}-Fc at approximately twice the amplitude of those for 11-Fc at equal concentrations. Both Fc-tagged proteins seemed to have reduced off-rates compared with the untagged monomers (Fig. 2A). A comparison of these data shows that dimerization by Fc tagging increased the molar affinity (K_D) of WT domain 11 for IGF-II from 118.8 ± 3.5 to 3.26 ± 0.3 nmol/L and the affinity of 11^{E1544K} from 20.5 ± 2.0 to 1.79 ± 0.08 nmol/L (Table 2). The 11^{E1544K}-Fc had the highest affinity of all the proteins tested with the molar affinity of 11^{E1544K}-Fc approximately twice that of 11-Fc. The improvement in affinity of the Fc-tagged dimers compared with the monomers was largely due to a substantial decrease in the off-rate (k_{d1}), from 7.87 ± 0.29 × 10^{-2} s^{-1} to 0.445 ± 0.04 × 10^{-2} s^{-1} for 11-Fc and from 4.06 ± 0.28 × 10^{-2} s^{-1} to 0.401 ± 0.03 × 10^{-2} s^{-1} for 11^{E1544K}-Fc. Fc tagging approximately doubled the on-rate (k_{a1}) for WT domain 11 from 6.62 ± 0.13 × 10^5 mol/L^{-1} s^{-1} to 13.65 ± 0.01 × 10^5 mol/L^{-1} s^{-1} but had little effect on the on-rate for

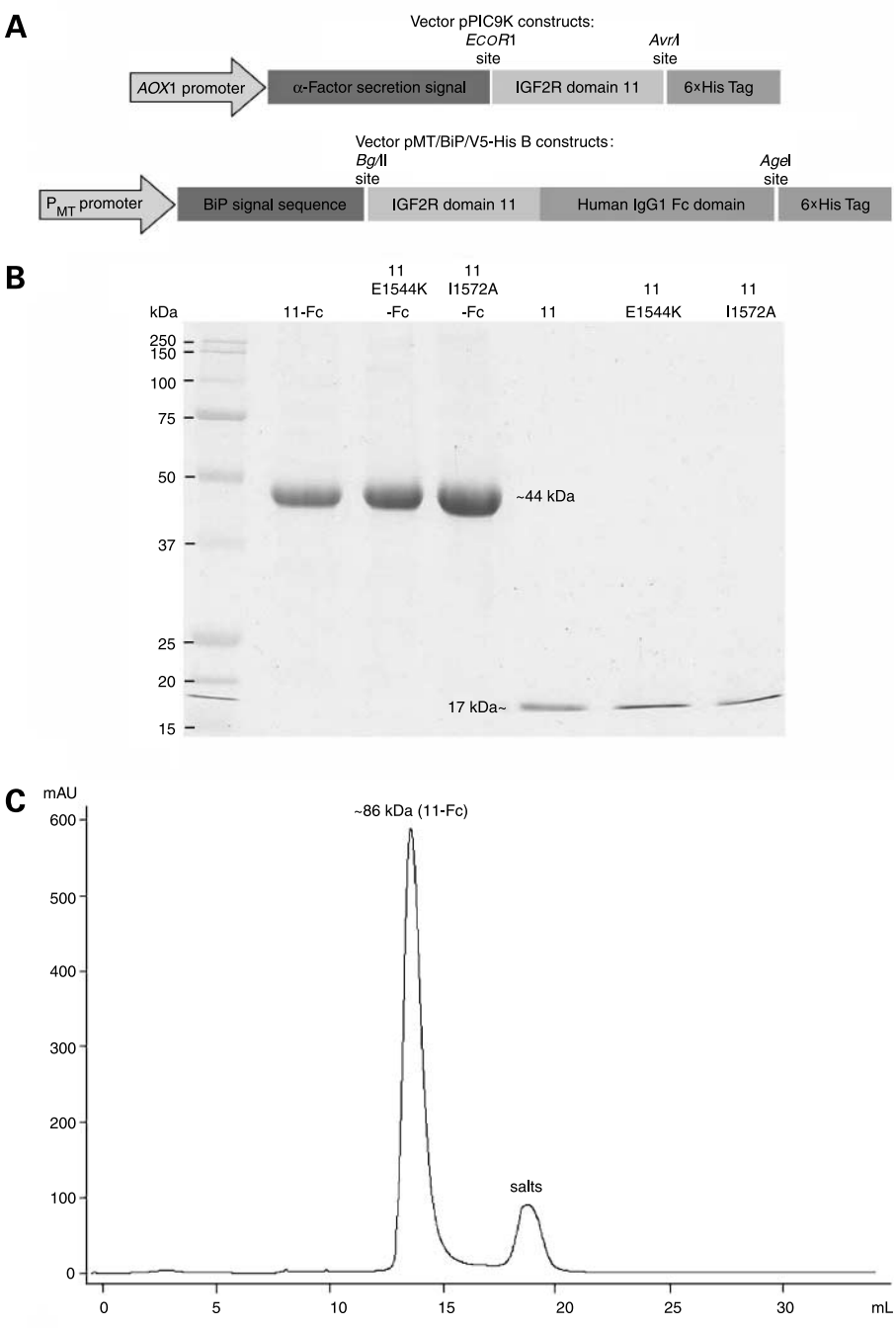

Figure 1. Protein expression and purification. **A,** domain 11 of human IGF2R was cloned into the expression vectors pPIC9K and pMT/BiP/V5-His B; the latter vector, including a COOH-terminal human IgG1 Fc tag for dimerization. **B,** mutations were introduced at IGF2R residues 1544 and 1572. Proteins 11-Fc, 11^{E1544K}-Fc, and 11^{I1572A}-Fc were expressed in *Drosophila* D.Mel-2 cells and purified via protein A-Sepharose affinity chromatography. The single domain proteins, WT domain 11, 11^{E1544K}, and 11^{I1572A} were expressed in *P. pastoris* and purified via nickel affinity chromatography. Aliquots of eluate (10 μL) were electrophoresed on 12% SDS-PAGE under reducing conditions and Coomassie stained. **C,** Fc-tagged proteins were further purified under nondenaturing conditions via a gel filtration column calibrated against protein standards. Representative A_{280} nm elution trace for 11-Fc.

11^{E1544K}, which remained high at 22.27 ± 0.74 × 10^5 mol/L^{-1} s^{-1} (Table 2). However, the substantially higher on-rate of 11^{E1544K}-Fc compared with 11-Fc seemed to account for its higher molar affinity. The molar affinity of the Fc-tagged proteins was considered too high to verify by isothermal titration calorimetry, as isothermal titration calorimetry cannot be easily used to measure affinities higher than 10 nmol/L. Minor kinetic variables were also obtained from the sensogram data (Table 2) but were too small to show any significant formation of the AB2 complex, where the analyte can form a bridge across two ligand molecules. This second binding event is purely a function of ligand immobilization. This is an example of a linked reaction, where the formation of the AB2 complex is entirely dependent on the prior formation of AB, and that to dissociate, the AB2 must first decay back to AB. From the fits, the calculated R_{max} for the Fc-tagged proteins was approximately 75% to 85% of the theoretical R_{max} (286 resonance units) and we concluded that a high percentage of the Fc-tagged proteins was therefore functional.

Table 1. Calculated masses, isoelectric points, and molar extinction coefficients of the proteins studied

Protein	Molecular weight (kDa)	pI	Extinction coefficient (mol/L^{-1} cm^{-1} at 280 mm)
$11^{wild\text{-}type}$	16.82	7.76	13,650
11^{E1544K}	16.82	8.45	13,650
11^{I1572A}	16.77	7.76	13,650
$11^{wild\text{-}type}$-Fc	88.06	8.02	94,420
11^{E1544K}	88.06	8.36	94,420
11^{I1572A}	87.98	8.02	94,420

Abbreviation: pI, isoelectric point.

Control for Mass Transfer Limitation

To confirm the absence of a mass transfer limitation, we did a control experiment, whereby binding reactions at different flow rates were compared (Fig. 2C and D). The 11^{E1544K}-Fc protein was injected over the IGF-II surface at a concentration of 0.616 nmol/L and at flow rates of 5, 20, 40, 60, and 75 μL per min. By varying the flow rates, limitations on the rate of transfer of 11^{E1544K}-Fc between bulk solution and the sensor chip surface were identifiable. The binding profiles obtained (Fig. 2C) represented differences in amplitude of <5% between the three highest flow rates. Further, the binding profiles seemed to plateau toward the highest flow rates (Fig. 2D). The data presented here show minimal mass transfer effects even at the low concentration of analyte used, where mass transfer would be expected to have its greatest effect. From these data, we conclude that mass transfer at a flow rate of 75 μL per min (the flow rate used for the kinetic experiments) had a minimal effect on the calculation of binding kinetics.

Ability of the Domain 11 Constructs to Block Functional Activity of IGF-II *In vitro*

We next investigated the ability of the domain 11 proteins to inhibit the actions of IGF-II *in vitro*, by

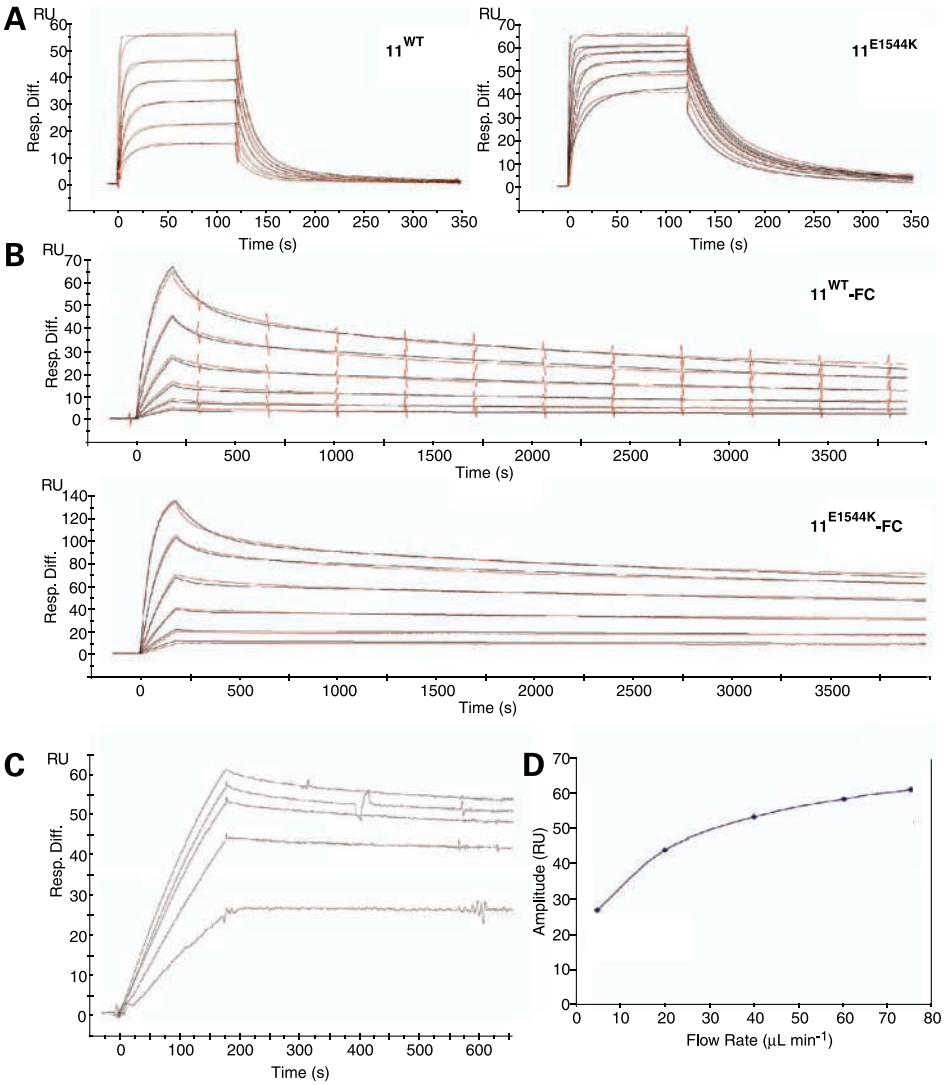

Figure 2. Binding of Fc-tagged and untagged domain 11 proteins to IGF-II. **A,** non-Fc-tagged proteins were injected over an IGF-II–coated BIAcore SA sensor chip flow cell surface at a flow rate of 40 μL min^{-1} and a range of concentrations (32, 64, 128, 256, 512, and 2048 nmol/L). Association was for 2 min and dissociation was for 4 min. Data from buffer controls and a reference flow cell were subtracted and data were fitted to a two-state conformational change model using BIAevaluation software. Data were from Zaccheo et al.(44). Representative fitted sensorgrams for WT domain 11 (11^{WT}; *left*) and domain 11^{E1544K} (*right*). **B,** Fc-tagged proteins were injected over the same chip at a flow rate of 75 μL min^{-1} and a different range of concentrations (2.464, 1.232, 0.616, 0.308, 0.154, and 0.077 nmol/L). Association was for 3 min and dissociation was for 60 min. Data from buffer controls and a reference flow cell were subtracted and data were fitted to a bivalent analyte model using BIAevaluation software. Representative fitted sensorgrams for 11^{WT}-Fc (*top*) and 11^{E1544K}-Fc (*bottom*). **C** and **D,** control for mass transfer limitation. Protein 11^{E1544K}-Fc was injected over an IGF-II–coated BIAcore SA sensor chip flow cell surface at 0.616 nmol/L at a range of flow rates (5, 20, 40, 60, and 75 μL min^{-1}). Association was for 3 min and dissociation was for 60 min. Data were aligned using BIAevaluation software. **C,** aligned sensorgrams of the data. **D,** graph of flow rate versus amplitude of binding.

Table 2. Kinetic and affinity constants for IGF-II binding to IGF2R domain 11 proteins studied

Protein	Major kinetic variables			Minor kinetic variables		
	k_{a1} ($\times 10^5$ mol/L^{-1} s^{-1})	k_{d1} ($\times 10^{-2}$ s^{-1})	K_D ($\times 10^{-9}$ mol/L)	k_{a2} ($\times 10^{-3}$ s^{-1})	k_{a2} ($\times 10^{-5}$ RU^{-1} s^{-1})	k_{d2} ($\times 10^{-4}$ s^{-1})
$11^{\text{wild-type}}$	6.62 ± 0.13	7.87 ± 0.29	118.8 ± 3.5	2.45 ± 0.33	—	121 ± 7.2
11^{E1544K}	20.23 ± 2.97	4.06 ± 0.28	20.5 ± 2.0	3.83 ± 1.10	—	79 ± 28
11^{I1572A}	—	—	—	—	—	—
$11^{\text{wild-type}}$-Fc	13.65 ± 0.01	0.445 ± 0.04	3.26 ± 0.3	—	7.12 ± 0.19	2.33 ± 0.12
11^{E1544K}	22.27 ± 0.74	0.401 ± 0.03	1.79 ± 0.08	—	7.86 ± 0.04	1.26 ± 0.03
11^{I1572A}	—	—	—	—	—	—

NOTE: The values given correspond to the average value ± the SE of three independent experiments. We have published the kinetic constants for non-Fc-tagged domain 11 proteins previously (44).
Abbreviation: RU, resonance unit.

assessing the phosphorylation of downstream targets of IGF1R signaling and IGF-II–induced proliferation as measured by [^{3}H]thymidine incorporation into nascent DNA. We used two different cell lines, HaCaT human keratinocytes, which have been shown previously to proliferate in response to IGF-II (48, 49), and immortalized *Igf2*$^{-/-}$ MEFs, generated using a 3T3 protocol from an inbred 129S2 mouse line (50). Addition of IGF-II for 10 min to serum-starved HaCaT cells or *Igf2*$^{-/-}$ MEFs lead to an increase in the phosphorylation of PKB in a dose-dependent manner (Fig. 3A and B). In *Igf2*$^{-/-}$ MEFs, a similar dose response pattern was observed for phosphorylation of MAPK (Thr^{202}/Tyr^{204}). However, a high basal level of activation was observed in HaCaT cells in serum-free medium with no further phosphorylation of MAPK on addition of IGF-II for 10 min under our experimental conditions (data not shown). This precluded use of this marker as an IGF-II–dependent activation assay. Stimulation of cells with increasing concentrations of IGF-II for 24 h stimulated DNA synthesis, also in a dose-dependent manner (Fig. 3C and D). Subsequent experiments were done using 1.3 nmol/L IGF-II for signaling experiments and 6.5 nmol/L IGF-II for proliferation experiments, as these concentrations of IGF-II gave consistent maximal stimulation.

The domain 11 constructs $11^{\text{wild-type}}$, 11^{E1544K} (enhanced mutation), 11^{E1572A} (null mutation) 11-Fc, 11^{E1544K}-Fc, and 11^{E1572A}-Fc were investigated for their ability to block IGF-II–stimulated proliferation and signaling in *Igf2*$^{-/-}$MEFs. Of the different constructs, only the Fc-tagged enhanced mutant (11^{E1544K}-Fc) showed significant ability to inhibit IGF-II–stimulated proliferation and activation of the IGF1R

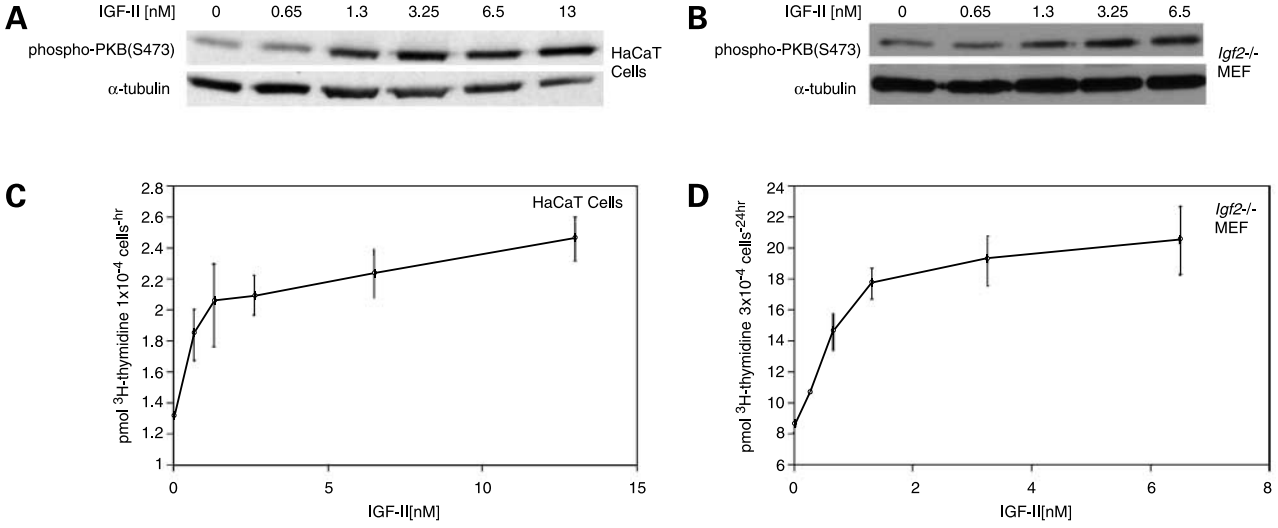

Figure 3. IGF-II dose-dependent increase in phosphorylation of PKB and cell proliferation. **A,** HaCaT; **B,** MEF. Increasing doses of IGF-II lead to an increase in phosphorylation of PKB in immortalized MEFs homozygous null for *Igf2* (*Igf2*$^{-/-}$) and HaCaT cell lines. Samples were probed with an anti–phospho-(Ser^{473}) PKB antibody. Equal loading was confirmed by reprobing the blot with an antibody to α-tubulin. Increasing doses of IGF-II lead to an increase in cell proliferation as measured by [^{3}H]thymidine incorporation in HaCaT cells (**C**) and *Igf2*$^{-/-}$ MEFs (**D**). The experiment was done at least thrice with each dose done in triplicate. *Points,* mean; *bars,* SE.

(Fig. 4). When equivalent numbers of IGF-II binding sites were present for the single 11^{E1544K} domain, compared with the Fc-tagged homodimer, only 11^{E1544K}-Fc could inhibit IGF-II–mediated activation of the cells significantly, although it seems that both proliferation and signaling are slightly attenuated by 11^{E1544K} (Fig. 4A and B). 11^{E1544K}-Fc was also the construct with the highest measured affinity for IGF-II (Table 2).

The inhibitory properties of 11^{E1544K}-Fc were further investigated by assessing its ability to inhibit IGF-II–dependent proliferation in HaCaT cells (Fig. 5). Keeping the concentration of IGF-II constant (6.5 nmol/L), we found that 11^{E1544K}-Fc decreased the ability of IGF-II to stimulate proliferation in a dose-dependent manner, with 650 and 1300 nmol/L significantly decreasing proliferation by 50% ($P = 0.005$) and 73% ($P = 0.013$), respectively (Fig. 5A). When the decrease in [^{3}H]thymidine uptake was equated to the concentration of functional IGF-II remaining in the medium, 650 and 1,300 nmol/L 11^{E1544K}-Fc reduced the amount of active IGF-II by 82% and 90%, respectively (Fig. 5A, *inset*).

Compared with 11^{E1544K}-Fc, the Fc-tagged null mutant (11^{I1572A}-Fc) that had no affinity for IGF-II was unable to inhibit either IGF-II–stimulated proliferation (Fig. 5B) or stimulation of IGF1R activation as measured by phosphorylation of PKB (AKT; Fig. 5C). This suggests that the ability of 11^{E1544K}-Fc to inhibit the actions of IGF-II is dependent on its capacity to bind directly to the ligand. In addition, 11^{E1544K}-Fc inhibitory function was specific for IGF-II, as it was unable to block the actions of IGF-I either on proliferation (Fig. 5B) or stimulation via IGF1R (Fig. 5C). Overall, the surface plasmon resonance results combined with functional assays indicate that 11^{E1544K}-Fc is both highly specific for IGF-II and that its inhibitory potency reflects its enhanced affinity for the IGF-II ligand.

Discussion

Native IGF2R is too large and complex to mass produce, and so we have manipulated domain 11 to make a stable, soluble chimeric Fc-tagged protein with high affinity for IGF-II that is similar to the affinity and selectivity of the full-length version of the protein (36, 44). When expressed as a fusion protein with human IgG1 Fc, the homodimer that is generated has the potential added advantages of increased valency, stability *in vivo* and clearance of trap and ligand via Fc(Rn) receptors, and enhanced complement activation (51).

Targeted mutagenesis of the AB, CD, and FG loops of the IGF-II ligand binding site of IGF2R domain 11 led us to the identification of a second sphere residue in the AB loop, which when mutated from glutamic acid to lysine increased the affinity of monomeric domain 11 by 6-fold (44). However, as a domain 11 monomer, this construct was not functionally active as an IGF-II antagonist *in vitro*, even at high molar ratio with respect to IGF-II (200:1). Increasing the valency of a protein is a further mechanism that can result in the enhanced functional affinity (avidity). Here,

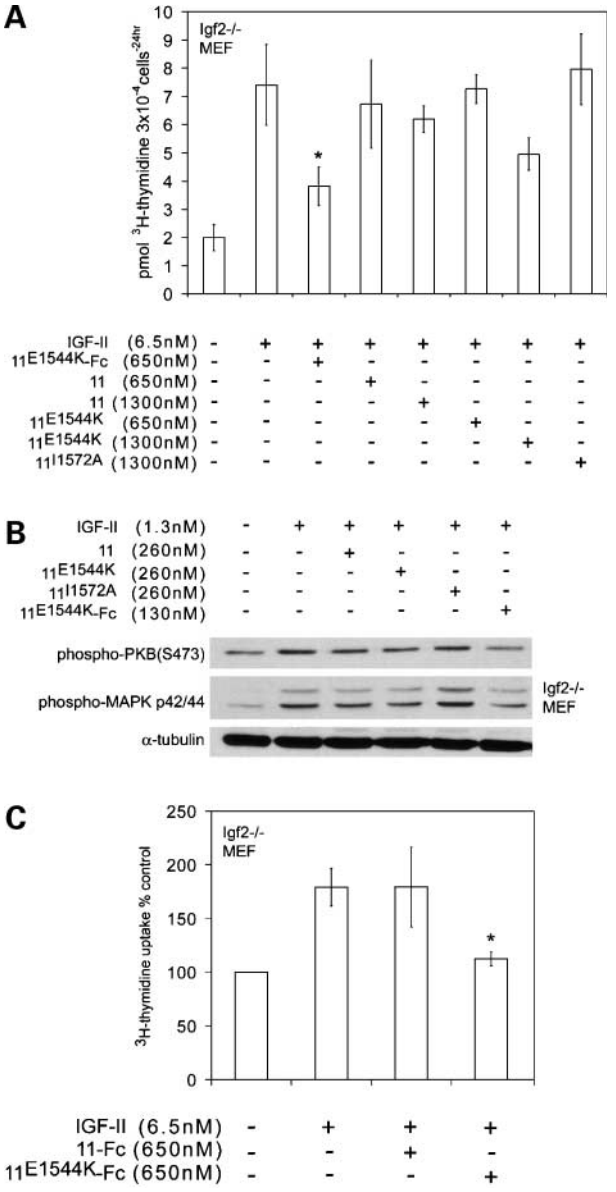

Figure 4. Inhibition of IGF-II–induced signaling and cell proliferation by domain 11 ligand traps. Domain 11 constructs with two different mutations, E1544K (which enhances IGF-II binding) and I1572A (which inhibits IGF-II binding), either with or without an Fc tag, were compared in their ability to block the actions of IGF-II in $Igf2^{-/-}$ MEFs. **A,** $Igf2^{-/-}$ MEFs were stimulated for 24 h with 6.5 nmol/L IGF-II preincubated for 10 min at room temperature with the domain 11 constructs indicated at 650 or 1,300 nmol/L (100-fold and 200-fold molar ratio, respectively). At 1,300 nmol/L, 11^{E1544K} had the equivalent number of IGF-II binding sites as 650 nmol/L 11^{E1544K}-Fc. However, only the homodimer, 11^{E1544K}-Fc, significantly decreased [^{3}H]thymidine incorporation compared with IGF-II alone. *Columns,* average ($n = 3$); *bars,* SE. *, $P = 0.04$. **B,** IGF-II–stimulated phosphorylation of PKB and MAPK was inhibited by preincubation with 11^{E1544K}-Fc only. Again, the domain 11 monomers were unable to inhibit the actions of IGF-II even with equivalent numbers of IGF-II binding sites present. Equal loading was confirmed by reprobing the blot with an anti–α-tubulin antibody. **C,** comparison of Fc homodimer proteins. The 11^{E1544K}-Fc construct significantly inhibited IGF-II–stimulated proliferation compared with 11-Fc, although the affinity for IGF-II is the same order of magnitude (see Table 2). *Columns,* mean ($n = 3$ experiments with triplicate samples); *bars,* SE. *, $P = 0.024$.

the relative affinity of purified bivalent versions of domain 11 protein determined *in vitro* directly correlates with the functional potency as antagonists of IGF-II–induced signaling and growth. The highest affinity construct, 11^{E1544K}-Fc, has an experimentally determined K_D of 1.79 nmol/L and was the only construct with the ability to reduce the molar equivalent dosage of IGF-II by at least 80% when added at 100-fold molar excess. Introduction of a mutation that stabilizes the ligand interaction by shortening the ''on-rate'' and prolonging the ''off-rate'' has made a substantial enhancement to the functional potency of the homodimer, although the WT domain 11-Fc construct has an affinity that is only 2-fold lower (3.26 nmol/L $11^{wildtype}$-Fc compared with 1.79 nmol/L 11^{E1544K}-Fc). This result also suggests that functional potency may also be determined by the relative affinity of the trap to IGF1R and IGF binding proteins, which also have relative affinities for IGF-II in the low nanomolar range, similar to neutralizing anti-IGF-II antibodies (52).

The observation that at least a 10-fold excess receptor is required to inhibit function is not unlike previous results obtained for other functional ligand traps (53). Importantly, mathematical modeling of the competition for ligand by soluble ligand traps is nonlinear and suggests that complete inhibition of cell surface receptor binding may be achieved by a concentration of soluble trap at least four to eight orders of magnitude greater than the equilibrium dissociation constant (K_D) for ligand binding to surface receptors (54, 55). For the IGF1R/IGF-II interaction, the K_D is ~23 nmol/L when measured using BIAcore (56), suggesting the K_D of ~2 nmol/L for 11^{E1544K}-Fc at 200-fold excess would be predicted to be an inhibitor, shown by the 73% inhibition of IGF-II–dependent growth. Even so, further engineering of 11^{E1544K}-Fc may still be required to optimize *in vivo* potency.

Soluble cytokine and growth factor receptors occur naturally, usually following cleavage of extracellular domains, and have potential regulatory roles in several systems (57). Soluble ligand traps based on soluble receptors have been a successful mechanism to neutralize several different ligands in model systems and as therapeutics in disease (58–64). For example, soluble tumor necrosis factor receptor has been exploited as an inhibitor of inflammatory diseases, such as rheumatoid arthritis and inflammatory bowel disease, and clinical trials have shown efficacy and practical clinical benefit (65). Soluble transforming growth factor-β receptor type II has been developed and shown to have a negative regulatory role in transforming growth factor-β–mediated tumor growth (53, 66). The soluble vascular endothelial growth factor (VEGF)-Trap based on soluble forms of the VEGF receptor is a potent inhibitor of tumor growth, including established tumors, and is currently undergoing clinical trials (67, 68). Importantly, the engineered version of the VEGF-Trap exploits homodimerization to enhance inhibitory function and affinity using Fc of human IgG1. The first generation of Fc-VEGF receptor 1 constructs however still required further protein engineering, including deletion of a stretch of 10 basic amino acids and generation of chimeric VEGF receptor 1/VEGF receptor 2 Ig domains resulting in a higher affinity (1 pmol/L), improved *in vivo* kinetics, and stability leading to efficient blockade at 1.5 molar excess (67).

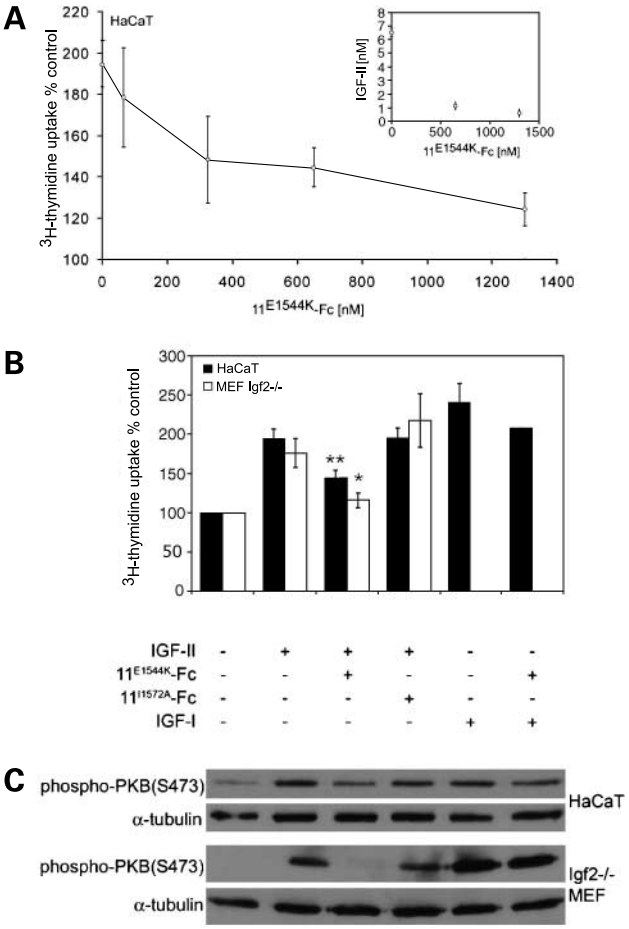

Figure 5. 11^{E1544K}-Fc decreases IGF-II–stimulated proliferation and signaling in a dose- and IGF-II–dependent manner. **A,** HaCaT cells were stimulated with 6.5 nmol/L IGF-II and increasing doses of 11^{E1544K}-Fc. A significant decrease in [^{3}H]thymidine incorporation was seen with 650 nmol/L (P = 0.005) and 1,300 nmol/L (P = 0.013) 11^{E1544K}-Fc. *Points,* average (n = 3 experiments with triplicate samples); *bars,* SE. *Inset,* the decrease in [^{3}H]thymidine uptake was equated to nanomol per liter of active IGF-II remaining. Six hundred fifty and 1,300 nmol/L IGF2R11^{E1544K}-Fc reduced proliferation by 50% and 73%, respectively, and the respective amount of active IGF-II was reduced by 82% and 90%. **B,** cells were stimulated with 6.5 nmol/L IGF-II or IGF-I and 650 nmol/L 11^{E1544K}-Fc or 11^{I1572A}-Fc. 11^{I1572A}-Fc failed to inhibit IGF-II–stimulated [^{3}H]thymidine incorporation in both HaCaT and immortalized *Igf2*$^{-/-}$ MEFs. IGF-I, which also stimulates [^{3}H]thymidine incorporation in HaCaT cells, was not inhibited by addition of 650 nmol/L 11^{E1544K}-Fc. 11^{E1544K}-Fc significantly inhibited IGF-II–stimulated proliferation in HaCaT cells (**, P = 0.005) and *Igf2*$^{-/-}$ MEFs (*, P = 0.034). *Columns,* average (n = 6 experiments with samples in triplicate); *bars,* SE. **C,** 11^{E1544K}-Fc blocks IGF-II–stimulated activation via the IGF1R. Cells were stimulated with 1.3 nmol/L IGF-II or IGF-I and 130 nmol/L 11^{E1544K}-Fc or 11^{I1572A}-Fc. 11^{E1544K}-Fc inhibited IGF-II–stimulated but not IGF-I–stimulated phosphorylation of PKB in HaCaT and *Igf2*$^{-/-}$ MEFs. 11^{I1572A}-Fc failed to inhibit IGF-II–stimulated phosphorylation. Equal loading was confirmed by reprobing the blots with an antibody to α-tubulin.

The actions of IGF-II *in vitro* can be blocked by purified soluble extracellular domains of IGF2R (69, 70), increased expression of full-length IGF2R can limit the growth of tumor xenografts (71, 72), and overexpression of soluble extracellular domain of IGF2R in the $Apc^{Min/+}$, $\Delta H19^{-m/+p}$ mouse model can reverse the tumor-promoting effects of biallelic expression of *Igf2 in vivo* (16). Alternative approaches that target deregulation of the IGF system in tumors include interruption of ligand receptor interactions by increasing the supply of binding proteins, introducing either ligand-specific or receptor antibodies (20, 52), expressing soluble and ligand binding forms of IGF1R (73), disruption of IGF1R receptor supply with RNA targeting (74), and inhibition of kinase activity of the IGF1R (75, 76). Each approach presents several practical problems (e.g., binding proteins may need to be modified to prevent proteolytic cleavage, antibody targeting of IGF1R may down-regulate both IGF1R and insulin receptor and induce feedback effects, targeting ubiquitously expressed IGF1R may result in systemic toxicity, and kinase inhibitor specificity may be a problem in view of the structural similarity with the insulin receptor).

The potential benefits for an IGF-II–specific therapeutic ligand trap include the targeting of IGF-II–producing regions of tumors, the subsequent inhibition of tumor progression and increased chemotherapy sensitivity in established human cancers, and as a novel therapeutic in nonislet cell tumor-related hypoglycemia.

Acknowledgments

We thank Chris Graham (Department of Zoology, University of Oxford, Oxford, United Kingdom), Yvonne Jones (Henry Wellcome Genomic Medicine, University of Oxford), and Mathew Crump (Department of Chemistry, University of Bristol, Bristol, United Kingdom) for discussion and Dellel Rezgui, Louise Falk, and Hefin Gill for help with experiments.

References

1. LeRoith D, Roberts CT, Jr. The insulin-like growth factor system and cancer. Cancer Lett 2003;195:127–37.

2. Foulstone E, Prince S, Zaccheo O, et al. Insulin-like growth factor ligands, receptors, and binding proteins in cancer. J Pathol 2005;205:145–53.

3. Pandini G, Frasca F, Mineo R, et al. Insulin/insulin-like growth factor I hybrid receptors have different biological characteristics depending on the insulin receptor isoform involved. J Biol Chem 2002;277:39684–95.

4. Baker J, Liu JP, Robertson EJ, Efstratiadis A. Role of insulin-like growth factors in embryonic and postnatal growth. Cell 1993;75:73–82.

5. Conover CA, Bale LK, Overgaard MT, et al. Metalloproteinase pregnancy-associated plasma protein A is a critical growth regulatory factor during fetal development. Development 2003;131:1187–94.

6. Martin DC, Fowlkes JL, Babic B, Khokha R. Insulin-like growth factor II signaling in neoplastic proliferation is blocked by transgenic expression of the metalloproteinase inhibitor TIMP-1. J Cell Biol 1999;146:881–92.

7. Miyamoto S, Yano K, Sugimoto S, et al. Matrix metalloproteinase-7 facilitates Insulin-like growth factor bioavailability through its proteinase activity on Insulin-like growth factor binding protein 3. Cancer Res 2004;64:665–71.

8. Hellawell GO, Turner GD, Davies DR, et al. Expression of the type 1 insulin-like growth factor receptor is up-regulated in primary prostate cancer and commonly persists in metastatic disease. Cancer Res 2002;62:2942–50.

9. Sell C, Rubini M, Rubin R, et al. Simian virus 40 large tumour antigen is unable to transform mouse embryonic fibroblasts lacking type I Insulin-like growth factor receptor. Proc Natl Acad Sci U S A 1993;90:11217–21.

10. Christofori G, Naik P, Hanahan D. A second signal supplied by insulin-like growth factor II in oncogene-induced tumorigenesis. Nature 1994;369:414–8.

11. Christofori G, Naik P, Hanahan D. Deregulation of both imprinted and expressed alleles of the insulin-like growth factor 2 gene during β-cell tumorigenesis. Nat Genet 1995;10:196–201.

12. Bates P, Fisher R, Ward A, et al. Mammary cancer in transgenic mice expressing insulin-like growth factor II (IGF-II). Br J Cancer 1995;72:1189–93.

13. Haddad R, Held WA. Genomic imprinting and Igf2 influence liver tumorigenesis and loss of heterozygosity in SV40 T antigen transgenic mice. Cancer Res 1997;57:4615–23.

14. Hahn H, Wojnowski L, Specht K, et al. Patched target Igf2 is indispensable for the formation of medulloblastoma and rhabdomyosarcoma. J Biol Chem 2000;275:28341–4.

15. Sakatani T, Kaneda A, Iacobuzio-Donahue CA, et al. Loss of imprinting of Igf2 alters intestinal maturation and tumorigenesis in mice. Science 2005;307:1976–8.

16. Harper J, Burns JL, Foulstone EJ, et al. Soluble IGF2 receptor rescues Apc(Min/+) intestinal adenoma progression induced by Igf2 loss of imprinting. Cancer Res 2006;66:1940–8.

17. Hassan AB, Howell JA. Insulin-like growth factor II supply modifies growth of intestinal adenoma in Apc(Min/+) mice. Cancer Res 2000;60:1070–6.

18. Sun Y, Gao D, Liu Y, et al. IGF2 is critical for tumorigenesis by synovial sarcoma oncoprotein SYT-SSX1. Oncogene 2006;25:1042–52.

19. Liao Y, Abel U, Grobholz R, et al. Up-regulation of insulin-like growth factor axis components in human primary prostate cancer correlates with tumor grade. Hum Pathol 2005;36:1186–96.

20. Sachdev D, Singh R, Fujita-Yamaguchi Y, Yee D. Down-regulation of insulin receptor by antibodies against the type I insulin-like growth factor receptor: implications for anti-insulin-like growth factor therapy in breast cancer. Cancer Res 2006;66:2391–402.

21. Lu L, Katsaros D, Wiley A, et al. The relationship of insulin-like growth factor-II, insulin-like growth factor binding protein-3, and estrogen receptor-α expression to disease progression in epithelial ovarian cancer. Clin Cancer Res 2006;12:1208–14.

22. Breuhahn K, Vreden S, Haddad R, et al. Molecular profiling of human hepatocellular carcinoma defines mutually exclusive interferon regulation and insulin-like growth factor II overexpression. Cancer Res 2004;64:6058–64.

23. Miyamoto S, Nakamura M, Shitara K, et al. Blockade of paracrine supply of insulin-like growth factors using neutralizing antibodies suppresses the liver metastasis of human colorectal cancers. Clin Cancer Res 2005;11:3494–502.

24. El-Badry OM, Minniti C, Kohn EC, et al. Insulin-like growth factor II acts as an autocrine growth and motility factor in human rhabdomyosarcoma tumors. Cell Growth Differ 1990;1:325–31.

25. Zhan S, Shapiro DN, Helman LJ. Loss of imprinting of IGF2 in Ewing's sarcoma. Oncogene 1995;11:2503–7.

26. Ravenel JD, Broman KW, Perlman EJ, et al. Loss of imprinting of insulin-like growth factor-II (IGF2) gene in distinguishing specific biologic subtypes of Wilms tumor. J Natl Cancer Inst 2001;93:1698–703.

27. Cui H, Cruz-Correa M, Giardiello FM, et al. Loss of IGF2 imprinting: a potential marker of colorectal cancer risk. Science 2003;299:1753–5.

28. Kohda M, Hoshiya H, Katoh M, et al. Frequent loss of imprinting of IGF2 and MEST in lung adenocarcinoma. Mol Carcinog 2001;31:184–91.

29. Jirtle RL. IGF2 loss of imprinting: a potential heritable risk factor for colorectal cancer. Gastroenterology 2004;126:1190–201.

30. Daughaday WH, Trivedi B, Baxter RC. Serum ''big insulin-like growth factor II'' from patients with tumor hypoglycemia lacks normal E-domain O-linked glycosylation, a possible determinant of normal propeptide processing. Proc Natl Acad Sci U S A 1993;90:5823–7.

31. Scott CD, Firth SM. The role of the M6P/IGF-II receptor in cancer: tumor suppression or garbage disposal? Horm Metab Res 2004;36:261–71.

32. Hassan AB. Keys to the hidden treasures of the mannose 6-phosphate/insulin-like growth factor 2 receptor. Am J Pathol 2003;162:3–6.

33. Ghosh P, Dahms NM, Kornfeld S. Mannose 6-phosphate receptors: new twists in the tale. Nat Rev Mol Cell Biol 2003;4:202–12.

34. Dennis PA, Rifkin DB. Cellular activation of latent transforming growth factor β requires binding to the cation-independent mannose 6-phosphate/insulin-like growth factor type II receptor. Proc Natl Acad Sci U S A 1991;88:580 – 4.

35. Devi GR, Byrd JC, Slentz DH, MacDonald RG. An insulin-like growth factor II (IGF-II) affinity-enhancing domain localized within extracytoplasmic repeat 13 of the IGF-II/mannose 6-phosphate receptor. Mol Endocrinol 1998;12:1661 – 72.

36. Linnell J, Groeger G, Hassan AB. Real time kinetics of insulin-like growth factor II (IGF-II) interaction with the IGF-II/mannose 6-phosphate receptor: the effects of domain 13 and pH. J Biol Chem 2001;276:23986 – 91.

37. DaCosta SA, Schumaker LM, Ellis MJ. Mannose 6-phosphate/insulin-like growth factor 2 receptor, a bona fide tumor suppressor gene or just a promising candidate? J Mammary Gland Biol Neoplasia 2000;5:85 – 94.

38. De Souza AT, Hankins GR, Washington MK, Orton TC, Jirtle RL. M6P/IGF2R gene is mutated in human hepatocellular carcinomas with loss of heterozygosity. Nat Genet 1995;11:447 – 9.

39. Hankins GR, De Souza AT, Bentley RC, et al. M6P/IGF2 receptor: a candidate breast tumor suppressor gene. Oncogene 1996;12:2003 – 9.

40. Jamieson TA, Brizel DM, Killian JK, et al. M6P/IGF2R loss of heterozygosity in head and neck cancer associated with poor patient prognosis. BMC Cancer 2003;3:4.

41. Olson LJ, Yammani RD, Dahms NM, Kim JJ. Structure of uPAR, plasminogen, and sugar-binding sites of the 300 kDa mannose 6-phosphate receptor. EMBO J 2004;23:2019 – 28.

42. Brown J, Esnouf RM, Jones MA, et al. Structure of a functional IGF2R fragment determined from the anomalous scattering of sulfur. EMBO J 2002;21:1054 – 62.

43. Roberts DL, Weix DJ, Dahms NM, Kim JJ. Molecular basis of lysosomal enzyme recognition: three-dimensional structure of the cation-dependent mannose 6-phosphate receptor. Cell 1998;93:639 – 48.

44. Zaccheo OJ, Prince SN, Miller DM, et al. Kinetics of insulin-like growth factor II (IGF-II) interaction with domain 11 of the human IGF-II/mannose 6-phosphate receptor: function of CD and AB loop solvent-exposed residues. J Mol Biol 2006;359:403 – 21.

45. Wu AM, Tan GJ, Sherman MA, et al. Multimerization of a chimeric anti-CD20 single-chain Fv-Fc fusion protein is mediated through variable domain exchange. Protein Eng 2001;14:1025 – 33.

46. Hollister J, Conradt H, Jarvis DL. Evidence for a sialic acid salvaging pathway in lepidopteran insect cells. Glycobiology 2003;13:487 – 95.

47. Todaro GJ, Green H. Quantitative studies of the growth of mouse embryo cells in culture and their development into established lines. J Cell Biol 1963;17:299 – 313.

48. Kim HJ, Kim TY. IGF-II-mediated COX-2 gene expression in human keratinocytes through extracellular signal-regulated kinase pathway. J Invest Dermatol 2004;123:547 – 55.

49. Barreca A, De Luca M, Del Monte P, et al. *In vitro* paracrine regulation of human keratinocyte growth by fibroblast-derived insulin-like growth factors. J Cell Physiol 1992;151:262 – 8.

50. DeChiara TM, Efstratiadis A, Robertson EJ. A growth-deficiency phenotype in heterozygous mice carrying an insulin-like growth factor II gene disrupted by targeting. Nature 1990;345:78 – 80.

51. Kenanova V, Olafsen T, Crow DM, et al. Tailoring the pharmacokinetics and positron emission tomography imaging properties of anti-carcinoembryonic antigen single-chain Fv-Fc antibody fragments. Cancer Res 2005;65:622 – 31.

52. Feng Y, Zhu Z, Xiao X, et al. Novel human monoclonal antibodies to insulin-like growth factor (IGF)-II that potently inhibit the IGF receptor type I signal transduction function. Mol Cancer Ther 2006;5:114 – 20.

53. Komesli S, Vivien D, Dutartre P. Chimeric extracellular domain type II transforming growth factor (TGF)-β receptor fused to the Fc region of human immunoglobulin as a TGF-β antagonist. Eur J Biochem 1998;254:505 – 13.

54. Forsten KE, Lauffenburger DA. Interrupting autocrine ligand-receptor binding: comparison between receptor blockers and ligand decoys. Biophys J 1992;63:857 – 61.

55. Forsten KE, Lauffenburger DA. Autocrine ligand binding to cell receptors. Mathematical analysis of competition by solution ''decoys.'' Biophys J 1992;61:518 – 29.

56. Forbes BE, Hartfield PJ, McNeil KA, et al. Characteristics of binding of insulin-like growth factor (IGF)-I and IGF-II analogues to the type 1 IGF receptor determined by BIAcore analysis. Eur J Biochem 2002;269:961 – 8.

57. Levine SJ. Mechanisms of soluble cytokine receptor generation. J Immunol 2004;173:5343 – 8.

58. Duan DS, Werner S, Williams LT. A naturally occurring secreted form of fibroblast growth factor (FGF) receptor 1 binds basic FGF in preference over acidic FGF. J Biol Chem 1992;267:16076 – 80.

59. Honore P, Luger NM, Sabino MA, et al. Osteoprotegerin blocks bone cancer-induced skeletal destruction, skeletal pain, and pain-related neurochemical reorganization of the spinal cord. Nat Med 2000;6:521 – 8.

60. Asano Y, Yokoyama T, Shibata S, et al. Effect of the chimeric soluble granulocyte colony-stimulating factor receptor on the proliferation of leukemic blast cells from patients with acute myeloblastic leukemia. Cancer Res 1997;57:3395 – 7.

61. Taguchi A, Blood DC, del Toro G, et al. Blockade of RAGE-amphoterin signalling suppresses tumour growth and metastases. Nature 2000;405:354 – 60.

62. Pitti RM, Marsters SA, Lawrence DA, et al. Genomic amplification of a decoy receptor for Fas ligand in lung and colon cancer. Nature 1998;396:699 – 703.

63. Brantley DM, Cheng N, Thompson EJ, et al. Soluble Eph A receptors inhibit tumor angiogenesis and progression *in vivo*. Oncogene 2002;21:7011 – 26.

64. Peters K, Werner S, Liao X, et al. Targeted expression of a dominant negative FGF receptor blocks branching morphogenesis and epithelial differentiation of the mouse lung. EMBO J 1994;13:3296 – 301.

65. Moreland LW, Baumgartner SW, Schiff MH, et al. Treatment of rheumatoid arthritis with a recombinant human tumor necrosis factor receptor (p75)-Fc fusion protein. N Engl J Med 1997;337:141 – 7.

66. Muraoka RS, Dumont N, Ritter CA, et al. Blockade of TGF-β inhibits mammary tumor cell viability, migration, and metastases. J Clin Invest 2002;109:1551 – 9.

67. Holash J, Davis S, Papadopoulos N, et al. VEGF-Trap: a VEGF blocker with potent antitumor effects. Proc Natl Acad Sci U S A 2002;99:11393 – 8.

68. Fukasawa M, Korc M. Vascular endothelial growth factor-trap suppresses tumorigenicity of multiple pancreatic cancer cell lines. Clin Cancer Res 2004;10:3327 – 32.

69. Scott CD, Ballesteros M, Madrid J, Baxter RC. Soluble insulin-like growth factor-II/mannose 6-P receptor inhibits deoxyribonucleic acid synthesis in cultured rat hepatocytes. Endocrinology 1996;137:873 – 8.

70. Scott CD, Weiss J. Soluble insulin-like growth factor II/mannose 6-phosphate receptor inhibits DNA synthesis in insulin-like growth factor II sensitive cells. J Cell Physiol 2000;182:62 – 8.

71. Lee JS, Weiss J, Martin JL, Scott CD. Increased expression of the mannose 6-phosphate/insulin-like growth factor-II receptor in breast cancer cells alters tumorigenic properties *in vitro* and *in vivo*. Int J Cancer 2003;107:564 – 70.

72. O'Gorman DB, Weiss J, Hettiaratchi A, Firth SM, Scott CD. Insulin-like growth factor-II/mannose 6-phosphate receptor overexpression reduces growth of choriocarcinoma cells *in vitro* and *in vivo*. Endocrinology 2002;143:4287 – 94.

73. D'Ambrosio C, Ferber A, Resnicoff M, Baserga R. A soluble insulin-like growth factor I receptor that induces apoptosis of tumor cells *in vivo* and inhibits tumorigenesis. Cancer Res 1996;56:4013 – 20.

74. Bohula EA, Playford MP, Macaulay VM. Targeting the type 1 insulin-like growth factor receptor as anti-cancer treatment. Anticancer Drugs 2003;14:669 – 82.

75. Mitsiades CS, Mitsiades NS, McMullan CJ, et al. Inhibition of the insulin-like growth factor receptor 1 tyrosine kinase activity as a therapeutic strategy for multiple myeloma, other hematologic malignancies, and solid tumours. Cancer Cell 2004;5:221 – 30.

76. Gacia-Echevrria C, Pearson M, Marti A, et al. *In vivo* antitumour activity of NVP-AEW41—a novel, potent, and selective inhibitor of the IGF-1R kinase. Cancer Cell 2004;5:231 – 9.

Molecular Cancer Therapeutics

Functional evaluation of novel soluble insulin-like growth factor (IGF)-II–specific ligand traps based on modified domain 11 of the human IGF2 receptor

Stuart N. Prince, Emily J. Foulstone, Oliver J. Zaccheo, et al.

Mol Cancer Ther 2007;6:607-617.